

MixGRPO: Unlocking Flow-based GRPO Efficiency with Mixed ODE-SDE

Junzhe Li^{1,2,3*}, Yutao Cui^{1*}, Tao Huang^{1*}, Yingping Ma³, Chun Fan³,
Miles Yang¹, Zhao Zhong^{1†}, Liefeng Bo¹,

¹ Hunyuan, Tencent,

² School of Computer Science, Peking University,

³ Computer Center, Peking University

Abstract

Although GRPO substantially enhances flow matching models in human preference alignment of image generation, methods such as FlowGRPO and DanceGRPO still exhibit inefficiency due to the necessity of sampling and optimizing over all denoising steps specified by the Markov Decision Process (MDP). In this paper, we propose **MixGRPO**, a novel framework that leverages the flexibility of mixed sampling strategies through the integration of stochastic differential equations (SDE) and ordinary differential equations (ODE). This streamlines the optimization process within the MDP to improve efficiency and boost performance. Specifically, MixGRPO introduces a sliding window mechanism, using SDE sampling and GRPO-guided optimization only within the window, while applying ODE sampling outside. This design confines sampling randomness to the time-steps within the window, thereby reducing the optimization overhead, and allowing for more focused gradient updates to accelerate convergence. Additionally, as time-steps beyond the sliding window are not involved in optimization, higher-order solvers are supported for faster sampling. So we present a faster variant, termed **MixGRPO-Flash**, which further improves training efficiency while achieving comparable performance. MixGRPO exhibits substantial gains across multiple dimensions of human preference alignment, outperforming DanceGRPO in both effectiveness and efficiency, with nearly 50% lower training time. Notably, MixGRPO-Flash further reduces training time by 71%.¹

1. Introduction

Recent advances [17, 18, 42, 43, 49] in Text-to-Image (T2I) tasks have demonstrated that probability flow models can achieve improved performance by incorporating Reinforce-

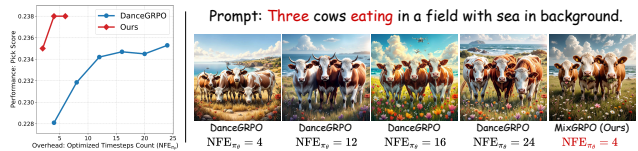


Figure 1. Comparison of our MixGRPO and DanceGRPO with **varying denoising steps to be optimized**. MixGRPO achieves higher performance with lower overhead.

ment Learning from Human Feedback (RLHF) [25] strategies during the post-training stage to maximize rewards. Specifically, methods [17, 43] based on Group Relative Policy Optimization (GRPO) [32], have recently been studied, achieving optimal alignment with human preferences.

Current GRPO methods in probability flow models, such as Flow-GRPO and DanceGRPO, combine a rollout phase followed by an online optimization phase. During rollouts, they employ Stochastic Differential Equation (SDE) sampling at each denoising step to introduce randomness, thereby enabling the stochastic exploration required by RLHF. This allows the entire denoising process to be framed as a Markov Decision Process (MDP) in a stochastic environment, where GRPO is then applied to optimize the complete state-action sequence in the online optimization phase. However, the requirement to optimize the entire denoising steps introduces two challenges, *prohibitive computational overhead* and *unfocused and inefficient optimization*. i) The overhead arises because computing the policy ratio requires separate full-trajectory sampling from both the old ($\pi_{\theta_{old}}$) and new policies (π_{θ}). Although DanceGRPO proposes a workaround by optimizing a random subset of steps, our findings in Figure 1 reveal a critical trade-off: reducing the subset size to save computation severely compromises model performance. ii) Early-step gradients prioritize global structure while late-step gradients focus on fine details, leading to conflicting update signals. This may result in an inefficient training process.

To address these issues, we propose MixGRPO, a method that optimizes a strategic subset of denoising steps

*Equal contribution. (lijunzhe1028@stu.pku.edu.cn)

† Corresponding authors.

¹Code is available in <https://github.com/Tencent-Hunyuan/MixGRPO>.

to drastically reduce computational overhead while ensuring a more focused and efficient optimization. Specifically, we employ a mixed ODE-SDE strategy, applying SDE sampling to a denoising sub-interval and Ordinary Differential Equations (ODE) sampling to the rest. Recently, Coefficients-Preserving Sampling (CPS) [37] was proposed as a more principled alternative to standard SDE sampling. Further details are provided in 12. The policy optimization is confined only to the stochastic SDE sub-interval. This interval operates as a sliding window, systematically advancing from low-SNR (signal-to-noise ratio) steps to high-SNR denoising steps as training progresses. This curriculum-based approach is conceptually analogous to temporal discounting in RL [2, 10, 26], as it prioritizes the optimization of initial, high-impact steps that establish global structure from a vast exploration space (Figure 2 Right), before progressively shifting focus to the refinement of local details. This selective optimization not only reduces the computational burden but also fosters a more dedicated exploration. Furthermore, this decoupling allows us to accelerate the deterministic ODE portions with fast solvers (*e.g.*, DPMSolver++ [22]), since their posterior distributions are irrelevant to the optimization, thereby reducing rollout time without compromising final image quality.

To evaluate the performance and efficiency of MixGRPO, we conduct comprehensive experiments by implementing our method within the frameworks of both FlowGRPO [17] and DanceGRPO [43]. We use a set of reward models (HPS-v2.1 [41], Pick Score [12], ImageReward [42], Unified Reward [38], etc) that serve as both training guidance and evaluation metrics. The evaluation compares single versus multi-RM guidance and assesses both in-domain and out-of-domain performance. Alongside performance, computational overhead is tracked via the number of function evaluations (NFE) and training time. Specifically, trained and evaluated on the HPDv2 dataset [41], MixGRPO outperforms DanceGRPO across all metrics, particularly improving the ImageReward [42] from 1.088 to 1.629, surpassing DanceGRPO’s score of 1.436, while generating images with enhanced semantic quality, aesthetics, and reduced distortion. Furthermore, MixGRPO reduces the training time of DanceGRPO by nearly 50%. In addition, MixGRPO-Flash utilizes DPMSolver++ [22] to accelerate the sampling of $\pi_{\theta_{old}}$, reducing training time by 71%.

To summarize, the key contributions are outlined below:

- We propose a mixed ODE-SDE framework for GRPO training with flow-based models. This approach alleviates computational overhead by confining the stochastic optimization to a specific sub-interval of the Markov Decision Process.
- We introduce an SDE sliding window to dynamically schedule the optimization steps. By guiding the optimization from broad exploration to fine-grained refinement,

this strategy significantly enhances performance.

- Our hybrid framework enables the use of high-order ODE solvers to accelerate the deterministic sampling of $\pi_{\theta_{old}}$ during GRPO training. This yields substantial speedups with negligible performance degradation.
- Comprehensive experiments across multiple frameworks demonstrate the versatility of MixGRPO. Our method consistently achieves substantial performance gains while significantly reducing training overhead, highlighting its broad applicability and effectiveness.

2. Related Work

2.1. RL For Image Generation

Inspired by Proximal Policy Optimization (PPO) [31], early works [3, 5, 6, 14] integrated reinforcement learning (RL) into diffusion models by optimizing the score function [34] through policy gradient methods, thereby enabling the generation of images that better align with human preferences. Subsequently, [36] introduced offline-Direct Preference Optimization (DPO) to T2I tasks for the first time. This allows diffusion models to directly learn from human feedback and validates its effectiveness on large-scale models. Due to the tendency of offline win-lose pair data to shift the model away from its original distribution, some works [15, 46] have adopted online methods, continuously adjusting sampling trajectories through step-aware preference models during training to achieve improved performance. Recently, GRPO-based works *e.g.*, [35], Flow-GRPO [17] and DanceGRPO [43], have elevated RL-enhanced image generation to new heights. Specifically, they introduced GRPO to flow matching models, allowing divergent sampling by transforming the ODE into an equivalent SDE. DanceGRPO [43] also identified the overhead caused by full-step optimization as a bottleneck and sought to address it by reducing or randomly selecting a subset. However, this approach does not fundamentally address the issue. We hope to delve into the essence of GRPO on the probability flow and provide deeper insights through mixed sampling techniques and optimization scheduling.

2.2. Sampling Methods for Probability Flow

The development of generative sampling began with DDPM [8], which used a slow, SDE-based probability flow requiring thousands of steps. To accelerate this, DDIM [33] introduced a deterministic ODE-based approach, reducing sampling steps to around 100. This SDE / ODE duality was later unified by score-based models [34], paving the way for higher-order ODE solvers like DPM-Solver [21, 22] that reduced steps to 10. Higher-performance solvers [47, 48] continue to be proposed; however, the gains are relatively marginal and have ultimately been replaced by the distillation method [30, 45]. Concurrently, flow matching mod-

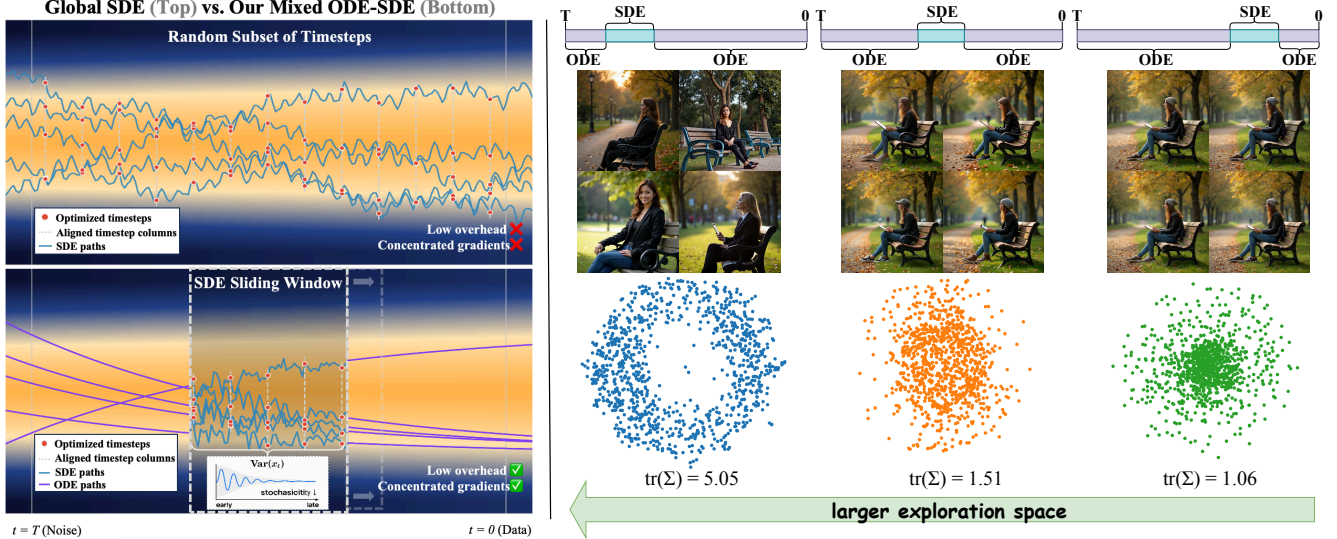


Figure 2. (Left) **Methods Comparison.** By employing the mixed ODE-SDE and sliding window strategy, MixGRPO reduces the number of optimized timesteps and achieves more efficient training than DanceGRPO [43]. (Right) **SDE Exploration Analysis.** As training progresses, MixGRPO gradually slides the SDE window from a high-noise to a low-noise regime, causing the exploration space to shrink and the distribution of sampled images to transition from dispersed to concentrated.

els [4, 16] simplified training by directly predicting the vector field, also enabling fast ODE sampling. Crucially, recent theoretical work [1, 7] has proven that flow matching and diffusion models share equivalent SDE and ODE formulations. This unification provides the theoretical foundation for our work, in which we explore an interleaved SDE and ODE sampling strategy within these probability flow models, thereby confining stochasticity to the SDE intervals in RL optimization, which shortens the effective MDP horizon and reduces training overhead.

3. Method

3.1. Mixed ODE-SDE Sampling in GRPO

According to Flow-GRPO [17], the SDE sampling in flow matching can be framed as a Markov Decision Process (MDP) $(\mathcal{S}, \mathcal{A}, \rho_0, P, \mathcal{R})$. The agent produces a trajectory during the discrete sampling process defined as $\Gamma = (s_0, \mathbf{a}_0, s_1, \mathbf{a}_1, \dots, s_T, \mathbf{a}_T)$, where the reward is provided only at the final step by the reward model, specifically $\mathcal{R}(s_i, \mathbf{a}_i) \triangleq R(\mathbf{x}_T, c)$ if $i = T$, and 0 otherwise.

In MixGRPO, we propose a sampling method that combines SDE and ODE. MixGRPO defines a time interval $S = [t_l, t_r] \subseteq [0, 1]$, which corresponds to a subset of denoising timesteps, such that $0 \leq l < r \leq T$ and $t_i = \frac{i}{T}$. We use SDE sampling within the interval S and ODE sampling outside, while S shifts along the denoising direction throughout the training process (See Figure 2 Left). MixGRPO restricts the stochastic exploration to the interval S , shortening the sequence length of the MDP to a subset $\Gamma_{\text{MixGRPO}} = (s_l, \mathbf{a}_l, s_{l+1}, \mathbf{a}_{l+1}, \dots, s_r, \mathbf{a}_r)$ and requires

reinforcement learning (RL) optimization only within S :

$$\max_{\theta} \mathbb{E}_{\Gamma_{\text{MixGRPO}} \sim \pi_{\theta}} \left[\sum_{t \in S} \left(\mathcal{R}(s_t, \mathbf{a}_t) - \beta D_{\text{KL}} \left(\pi(\cdot | s_t) \parallel \pi_{\text{ref}}(\cdot | s_t) \right) \right) \right], \quad (1)$$

MixGRPO reduces training overhead while also enabling more concentrated gradient updates. Next, we derive the specific sampling form and optimization objective.

For a deterministic reverse *probability flow ODE* [34], it takes the following form:

$$\frac{d\mathbf{x}_t}{dt} = f(\mathbf{x}_t, t) - \frac{1}{2} g^2(t) \nabla_{\mathbf{x}_t} \log q_t(\mathbf{x}_t), \quad (2)$$

where $q_t(\mathbf{x}_t)$ represents the evolution process of the reverse probability distribution from 0 to T . $\nabla_{\mathbf{x}_t} \log q_t(\mathbf{x}_t)$ is the *score function* at time t . According to the Fokker-Planck equation [24, 28], [34] has demonstrated that Eq. (2) has the following equivalent *probability flow SDE*, which maintains the same marginal distribution at each time t :

$$\frac{d\mathbf{x}_t}{dt} = f(\mathbf{x}_t, t) - g^2(t) \nabla_{\mathbf{x}_t} \log q_t(\mathbf{x}_t) + g(t) \frac{dw}{dt}. \quad (3)$$

In MixGRPO, we mix ODE and SDE for sampling, which has the same convergence as using only ODE sampling (a detailed proof in Supplementary). The specific form is as follows:

$$d\mathbf{x}_t = \begin{cases} [f(\mathbf{x}_t, t) - g^2(t) \mathbf{s}_t(\mathbf{x}_t)] dt + g(t) dw, & \text{if } t \in S, \\ [f(\mathbf{x}_t, t) - \frac{1}{2} g^2(t) \mathbf{s}_t(\mathbf{x}_t)] dt, & \text{otherwise,} \end{cases} \quad (4)$$

where we define the score function as $\mathbf{s}_t \triangleq \nabla_{\mathbf{x}_t} \log q_t(\mathbf{x}_t)$. In particular, for Flow Matching (FM) [16], especially the Rectified Flow (RF) [19], the sampling process can be viewed as a deterministic ODE:

$$\frac{d\mathbf{x}_t}{dt} = \mathbf{v}_t. \quad (5)$$

Eq. (5) is actually a special case of the Eq. (2) with $\mathbf{v}_t = f(\mathbf{x}_t, t) - \frac{1}{2}g^2(t)\mathbf{s}_t(\mathbf{x}_t)$. So we can derive mixed ODE-SDE sampling form for RF as follows:

$$d\mathbf{x}_t = \begin{cases} [\mathbf{v}_t - \frac{1}{2}g^2(t)\mathbf{s}_t(\mathbf{x}_t)] dt + g(t)d\mathbf{w}, & \text{if } t \in S, \\ \mathbf{v}_t dt, & \text{otherwise.} \end{cases} \quad (6)$$

In the RF framework, the model is used to predict the velocity field, represented as $\mathbf{v}_\theta(\mathbf{x}_t, t) = \frac{d\mathbf{x}_t}{dt}$. Following [17], the *score function* is represented as $\mathbf{s}_t(\mathbf{x}_t) = -\frac{\mathbf{x}_t}{t} - \frac{1-t}{t}\mathbf{v}_\theta(\mathbf{x}_t, t)$. The $g(t)$ is represented as the standard deviation of the noise $g(t) = \sigma_t$. According to the definition of the standard Wiener process, we use $d\mathbf{w} = \sqrt{dt}\epsilon$, where $\epsilon \sim \mathcal{N}(0, \mathbf{I})$. Applying Euler-Maruyama discretization for SDE and Euler discretization for ODE, we build the final denoising process in MixGRPO:

$$\mathbf{x}_{t+\Delta t} = \begin{cases} \mathbf{x}_t + \boldsymbol{\mu}_\theta(\mathbf{x}_t, t)\Delta t + \sigma_t\sqrt{\Delta t}\epsilon, & \text{if } t \in S, \\ \mathbf{x}_t + \mathbf{v}_\theta(\mathbf{x}_t, t)\Delta t, & \text{otherwise,} \end{cases} \quad (7)$$

where the SDE drift term for the sampling process is defined as $\boldsymbol{\mu}_\theta(\mathbf{x}_t, t) \triangleq \mathbf{v}_\theta(\mathbf{x}_t, t) + \frac{\sigma_t^2(\mathbf{x}_t + (1-t)\mathbf{v}_\theta(\mathbf{x}_t, t))}{2t}$. According to Eq. (1), we only need to optimize GRPO [32] at the time within the interval S for N samples in the group. For an unbiased advantage estimation in GRPO, we constrain the source of variation across images generated from a single prompt. Specifically, we fix the position of the SDE window, thereby sourcing all stochasticity from an identical timestep range in a GRPO group. This not only concentrates the gradients within this window but is also essential for preserving the unbiased nature of the optimization. The final training objective is represented as follows:

$$\mathcal{J}_{\text{MixGRPO}}(\theta) = \mathbb{E}_{c \sim \mathcal{C}, \{\mathbf{x}_t^i\}_{i=0}^N \sim \pi_{\theta_{\text{old}}}(\cdot|c)} \left[\frac{1}{N} \sum_{i=1}^N \frac{1}{|S|} \sum_{t \in S} \min \left(r_t^i(\theta) A^i, \text{clip} \left(r_t^i(\theta), 1 - \varepsilon, 1 + \varepsilon \right) A^i \right) - \beta \mathcal{J}_{\text{KL}} \right], \quad (8)$$

where ε is the clipping hyperparameter, $r_t^i(\theta)$ is the policy ratio, A^i is the advantage score and \mathcal{J}_{KL} is the KL-regularization, defined as follows:

$$\begin{aligned} r_t^i(\theta) &= \frac{q_\theta(\mathbf{x}_{t+\Delta t} | \mathbf{x}_t, c)}{q_{\theta_{\text{old}}}(\mathbf{x}_{t+\Delta t} | \mathbf{x}_t, c)}, \\ A^i &= \frac{R(\mathbf{x}_T^i, c) - \text{mean}(\{R(\mathbf{x}_T^i, c)\}_{i=1}^N)}{\text{std}(\{R(\mathbf{x}_T^i, c)\}_{i=1}^N)}, \\ \mathcal{J}_{\text{KL}} &= D_{\text{KL}}(\pi_\theta || \pi_{\theta_{\text{old}}}) = \frac{\|\mathbf{x}_{t+\Delta t}(\theta) - \mathbf{x}_{t+\Delta t}(\theta_{\text{old}})\|^2}{2\sigma_t^2 \Delta t}. \end{aligned} \quad (9)$$

Algorithm 1 MixGRPO Training Process

Require: initial policy model π_θ ; reward models $\{R_k\}_{k=1}^K$; prompt dataset \mathcal{C} ; total sampling steps T ; number of samples per prompt N ;

Require: sliding window $W(l)$, window size w , shift interval τ , window stride s

- 1: Init left boundary of $W(l)$: $l \leftarrow 0$
- 2: **for** training iteration $m = 1$ **to** M **do**
- 3: Sample batch prompts $\mathcal{C}_b \sim \mathcal{C}$
- 4: Update old policy model: $\pi_{\theta_{\text{old}}} \leftarrow \pi_\theta$
- 5: **for** each prompt $c \in \mathcal{C}_b$ **do**
- 6: Init the same noise $\mathbf{x}_0 \sim \mathcal{N}(0, \mathbf{I})$
- 7: **for** generate i -th image from $i = 1$ **to** N **do**
- 8: **for** sampling timestep $t = 0$ **to** $T - 1$ **do**
- 9: **if** $t \in W(l)$ **then**
- 10: Use SDE Sampling to get \mathbf{x}_{t+1}^i
- 11: **else**
- 12: Use ODE Sampling to get \mathbf{x}_{t+1}^i
- 13: **end if**
- 14: **end for**
- 15: **end for**
- 16: **for** i -th image from $i = 1$ **to** N **do**
- 17: Calculate advantages: $A_i \leftarrow \sum_{k=1}^K \frac{R(\mathbf{x}_T^i, c)_k^i - \mu_k}{\sigma_k}$
- 18: **end for**
- 19: **for** optimization timestep $t \in W(l)$ **do**
- 20: Update policy model: $\theta \leftarrow \theta + \eta \nabla_\theta \mathcal{J}$
- 21: **end for**
- 22: **end for**
- 23: **if** $m \bmod \tau$ is 0 **then** \triangleright move sliding window
- 24: $l \leftarrow \min(l + s, T - w)$
- 25: **end if**
- 26: **end for**

MixGRPO reduces the NFE of π_θ and optimized timesteps count compared to global SDE sampling. However, the NFE of $\pi_{\theta_{\text{old}}}$ is not reduced, as complete inference is required to obtain the final image for reward calculation. In Section 3.3, we will introduce the use of higher-order ODE solvers, which also reduce the NFE of $\pi_{\theta_{\text{old}}}$ leading to further speedup. In summary, the mixed ODE-SDE sampling significantly streamlines the MDP, enhancing training efficiency by lowering optimization overhead and enabling more focused gradient updates.

3.2. Sliding Window as Optimization Scheduler

In this section, we will introduce the sliding window to describe the movement of S , which leads to a significant improvement in the quality of the generated images. Along the denosing time-steps $\{0, 1, \dots, T - 1\}$, MixGRPO defines a SDE sliding window $W(l)$ and optimization is only employed at the timesteps within $W(l)$.

$$W(l) = \{t_l, t_{l+1}, \dots, t_{l+w-1}\}, \quad l \leq T - w, \quad (10)$$

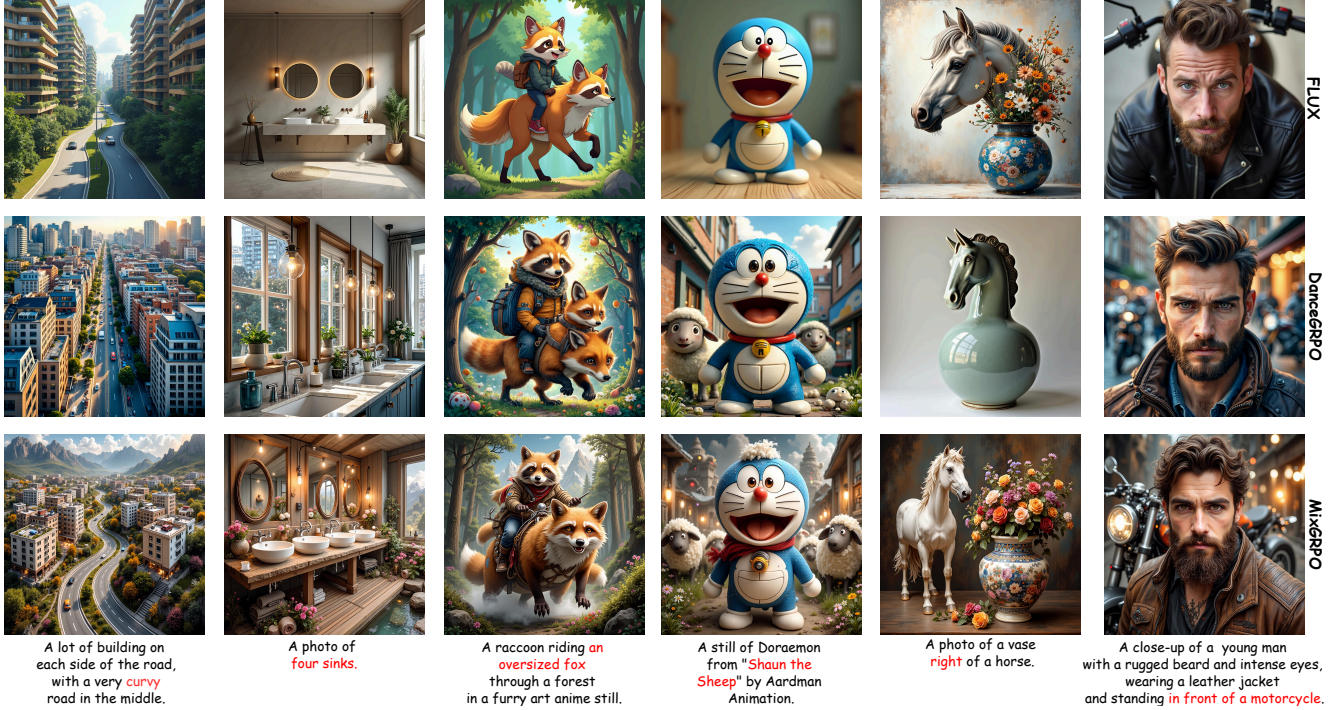


Figure 3. Qualitative comparison. MixGRPO achieve superior performance in semantics, aesthetics and text-image alignment.

where l is the *left boundary* of the sliding window, and w is a hyperparameter that represents the *window size*.

The *left boundary* l of the sliding window moves as the training progresses. The movement strategy of the sliding window is governed by the following parameters. τ is the shift interval, which specifies the number of training steps between each window shift. s is the window stride, which indicates the number of denoising timesteps that the left boundary l advances during each shift. The detailed sliding window strategy and MixGRPO algorithm can be found in Algorithm 1. In Section 4.4.1, we conduct thorough ablation studies to validate these parameters.

In our MixGRPO, the denoising process inherently follows a stochastic-to-deterministic trajectory: moving along the probability flow corresponds to a transition from high to low stochasticity, as illustrated in Figure 2 (right). Our sliding-window approach operationalizes this principle by creating an implicit training curriculum. This is analogous to reward shaping in RL [2, 10, 26], where discount factors prioritize rewards from the most critical steps in a process. For diffusion and flow-matching models, this curriculum directs the GRPO algorithm to first optimize low-SNR regions—where dynamics are highly stochastic—before shifting focus to the more deterministic, high-SNR regions for fine-grained refinement. This coarse-to-fine strategy stabilizes the initial, more volatile stages of training and enables the model to learn a robust global structure before perfecting finer details.

The experimental results of different movement strate-

gies in Table 4 demonstrate the validity of this intuition. Not only does the progressive strategy outperform random selection, but our findings also indicate that MixGRPO can achieve strong performance even with a static (frozen) window. In this setting, where optimization is exclusively applied to the initial timesteps, our method still surpasses DanceGRPO. This is because the initial timesteps in the generative process, which restores an image from Gaussian noise, account for a more substantial degree of denoising than other timesteps [4, 11]. Initial timesteps introduces greater stochasticity into the final output, thereby increasing the likelihood of generating images that align with the preferences of a reward model and ultimately yielding a higher optimization payoff. Based on this intuition, we also proposed an exponential decay strategy as follows, allowing τ to decrease as the window moves, enabling the model to avoid excessive optimization in smaller search spaces.

$$\tau(l) = \tau_0 \cdot \exp(-k \cdot \text{ReLU}(l - \lambda_{thr})), \quad (11)$$

where τ_0 is the initial shift interval, k is the decay factor, and λ_{thr} is the threshold that controls when the decay starts. The exponential function $\exp(x)$ calculates e^x , while the Rectified Linear Unit $\text{ReLU}(x)$ is defined as $\max(0, x)$. Table 4 shows that the exponential decay strategy can achieve better results in terms of Pick Score [12] and ImageReward [42]. This may be because the model focuses on the earlier stages of denoising, which can lead to more significant high-level changes, precisely what the human preference alignment reward model emphasizes.

3.3. Trade-off Between Overhead and Performance

Unlike DanceGRPO [43], which relies on global SDE sampling, MixGRPO employs a mixed ODE-SDE method, allowing the use of higher-order ODE solvers to accelerate GRPO training-time sampling. However, accelerating the ODE phase before the SDE window amplifies the solver’s numerical errors due to the window’s stochasticity, severely degrading image quality and corrupting the reward signal. In contrast, accelerating the ODE phase after the window provides a significant speed-up without compromising the image fidelity required for reliable reward evaluation. Therefore, MixGRPO exclusively accelerates the post-window ODE timesteps.

[7] has demonstrated the equivalence between the ODE sampling of flow matching models (FM) and DDIM, and Section 3.1 has also shown that diffusion probabilistic models (DPM) and FM share the same ODE form during the denoising process. Therefore, the higher-order ODE solvers *e.g.*, DPM-Solver Series [21, 22, 48], UniPC [47] designed for DPM sampling acceleration are also applicable to FM. We have reformulated DPM-Solver++ [22] to apply it in the FM framework for ODE sampling acceleration and released detailed derivations in Supplementary.

By applying higher-order solvers, we achieve acceleration in the sampling of $\pi_{\theta_{\text{old}}}$ during GRPO training, which is essentially a balance between overhead and performance. Excessive acceleration leads to fewer timesteps, which inevitably results in a decline in image generation quality, thereby accumulating errors in the computation of rewards. We have found in practice that the 2nd-order DPM-Solver++ is sufficient to provide significant acceleration while ensuring that the generated images align well with human preferences in Table 8.

Ultimately, we introduced DPM-Solver++ and adopted both progressive and frozen sliding window strategies, proposing MixGRPO-Flash and MixGRPO-Flash*. A detailed description of the algorithm can be found in Supplementary. These faster versions offer more substantial acceleration relative to base version of our MixGRPO, while simultaneously surpassing DanceGRPO in their alignment with human preferences.

4. Experiments

4.1. Experiment Setup

Dataset We conduct experiments using the prompts provided by the HPDV2 dataset, which is the official dataset for the HPS-v2 benchmark [41]. The training set contains 103,700 prompts; in fact, MixGRPO achieved good human preference alignment results after training one epoch with only 9,600 prompts. The test set consists of 400 prompts. The prompts are diverse, encompassing four styles: “Animation”, “Concept Art”, “Painting”, and “Photo”.

Model Following DanceGRPO [43], we use FLUX.1 Dev [13] as the base model, which is an advanced text-to-image model based on flow matching.

Overhead Evaluation For the evaluation of overhead, we use two metrics: the number of function evaluations (NFE) [21] and the time consumption per iteration during training. The NFE is divided into $\text{NFE}_{\pi_{\theta_{\text{old}}}}$ and $\text{NFE}_{\pi_{\theta}}$. $\text{NFE}_{\pi_{\theta_{\text{old}}}}$ represents the number of forward propagation of the reference model for computing the policy ratio and generating images. $\text{NFE}_{\pi_{\theta}}$ is the number of forward propagation of the policy model solely for the policy ratio. Additionally, the average training time per GRPO iteration provides a more accurate reflection of the acceleration effect.

Performance Evaluation We used four multiple reward models in conjunction for GRPO, namely HPS-v2.1 [41], Pick Score [12], ImageReward [42] and Unified Reward [38], both as reward guidance during training and as evaluation metrics. These metrics are all based on human preferences but emphasize different aspects. For example, ImageReward [42] highlights image-text alignment and fidelity, while Unified Reward [38] concentrates on semantics. DanceGRPO [43] also demonstrates that using multiple reward models can achieve better results. To validate the robustness of MixGRPO, we also followed DanceGRPO and conducted additional comparisons using HPS-v2.1 as a single reward, and combining HPS-v2.1 [41] and CLIP Score [27] as multi-rewards.

4.2. Implementation Details

For training-time sampling, we first perform a shift $\tilde{t} = \frac{t}{1-(\tilde{s}-1)t}$ on the uniformly distributed $t_i = \frac{i}{T}$ where $i = [0, \dots, T - 1]$, and then define $\sigma_t = \eta \sqrt{\frac{\tilde{t}}{1-\tilde{t}}}$. We set $\tilde{s} = 3$ and $\eta = 0.7$ as scale. We set $T = 25$ as the total sampling steps. For GRPO, the model generates 12 images for each prompt and clips the advantage to the range $[-5, 5]$. It is important to note that we use gradient accumulation over 3 steps, which means that during a single training iteration, there are $\frac{12}{3} = 4$ gradient updates. For the exponential decay strategy of the sliding window in Eq. (11), we empirically set $\tau_0 = 20$, $k = 0.1$, and $\lambda_{thr} = 13$. Furthermore, when multiple reward models are jointly trained with, each reward is assigned equal weight.

For training, all experiments are conducted on 32 Nvidia GPUs with a batch size per gpu of 1 and a maximum of 300 iterations. We use AdamW [20] as the optimizer with a learning rate of 1e-5 and a weight decay coefficient of 0.0001. Mixed precision training is used with the bfloat16 (bf16) format, while the master weights are maintained at fp32 precision. We also tried CPS sampling instead of normal SDE sampling, the details can be seen in 12.

Table 1. Comparison results for overhead and performance. MixGRPO achieves the best performance across multiple metrics. MixGRPO-Flash significantly reduces training time while outperforming DanceGRPO. **Bold**: rank 1. Underline: rank 2. *The Frozen strategy means that optimization is only employed at the initial denoising steps.

Method	NFE $_{\pi_{\theta_{old}}}$	NFE $_{\pi_{\theta}}$	Iteration Time (s) \downarrow	Human Preference Alignment			
				HPS-v2.1 \uparrow	Pick Score \uparrow	ImageReward \uparrow	Unified Reward \uparrow
FLUX	/	/	/	0.313	0.227	1.088	3.370
DanceGRPO	25	14	291.284	0.356	0.233	1.436	3.397
	25	4	149.978	0.334	0.225	1.335	3.374
	25	4*	150.059	0.333	0.229	1.235	3.325
MixGRPO	25	4	150.839	0.367	0.237	1.629	3.418
MixGRPO-Flash	16 (Avg)	4	<u>112.372</u>	<u>0.358</u>	<u>0.236</u>	1.528	<u>3.407</u>
	8	4*	83.278	0.357	0.232	<u>1.624</u>	3.402

Table 2. Comparison with DanceGRPO. The results demonstrate that MixGRPO achieves the best performance on both in-domain and out-of-domain rewards.

Reward Model	Method	In Domain		Out-of-Domain		
		HPS-v2.1	CLIP Score	Pick Score	ImageReward	Unified Reward
/	FLUX	0.313	0.388	0.227	1.088	3.370
HPS-v2.1	DanceGRPO	0.367	0.349	0.227	1.141	3.270
	MixGRPO	0.373	0.372	0.228	1.396	3.370
HPS-v2.1 & CLIP Score	DanceGRPO	0.346	0.400	0.228	1.314	3.377
	MixGRPO	0.349	0.415	0.229	1.416	3.430

4.3. Comparison with existing methods

To validate the generality, effectiveness, and efficiency of our proposed method, we conducted comprehensive experiments across two distinct frameworks: Dance-GRPO and Flow-GRPO. In our experiments, we employed multiple reward models for guidance, as described in Algorithm 1.

We first evaluated the overhead and performance of MixGRPO in comparison with DanceGRPO, with the results presented in Table 1. The official DanceGRPO uses $NFE_{\pi_{\theta}} = 14$; For fairness, we also tested DanceGRPO with $NFE_{\pi_{\theta}} = 4$. For MixGRPO-Flash, we evaluated both the progressive and frozen strategies, and to ensure fairness, we also applied the frozen strategy to DanceGRPO. The visual results are presented in Figure 3. We observe that MixGRPO achieves the best performance in terms of semantics, aesthetics, and text-image alignment. For a direct comparison at $NFE_{\pi_{\theta}} = 4$, the qualitative results are shown in Figure 4. confirms the robustness of acceleration in MixGRPO-Flash, demonstrating the model’s ability to preserve the aesthetic quality and semantic alignment while speeding up the process. Following DanceGRPO [43], we also trained and evaluated the model using a single reward model, e.g., HPSv2.1 and two reward models, e.g., HPSv2.1 and CLIP Score on the HPDv2 dataset [41]. The results (See Table 2) demonstrate that MixGRPO achieves the best performance on both in-domain and out-of-domain rewards, whether using a single or multiple reward models. The visualized results are displayed in Supplementary.

Methodologically, Flow-GRPO [17] and Dance-GRPO [43] are conceptually similar, differing only in minor aspects such as their sampling formulations and the

Table 3. Comparison with FlowDPO and FLOW-GRPO. The results demonstrate that MixGRPO outperforms others in training efficiency and performance.

Model	RL Method	NFE $_{\pi_{\theta_{old}}}$	NFE $_{\pi_{\theta}}$	HPSv2.1	Pick Score	ImageReward
SD3.5-M	/	/	/	0.3066	0.2266	1.1630
SD3.5-M+DPO LoRA	Offline DPO	40	40	0.3043	0.2220	1.4524
	Online DPO	40	40	0.3132	0.2210	1.5001
SD3.5-M+GRPO LoRA	Flow-GRPO	10	10	0.3312	0.2318	1.4572
	MixGRPO	10	4	0.3416	0.2360	1.4854

Table 4. Comparison for moving strategies.

Strategy	Interval Schedule	HPS-v2.1	Pick Score	ImageReward	Unified Reward
Frozen	/	0.354	0.234	1.580	3.403
Random	Constant	0.365	0.237	1.513	3.388
Progressive	Decay (Linear)	0.365	0.235	1.566	3.382
	Decay (Exp)	0.360	0.239	1.632	3.416
	Constant	0.367	0.237	1.629	3.418

Table 5. Comparison for different shift interval τ .

τ	HPS-v2.1	Pick Score	ImageReward	Unified Reward
15	0.366	0.237	1.509	3.403
20	0.366	0.238	1.610	3.411
25	0.367	0.237	1.629	3.418
30	0.350	0.229	1.589	3.385

use of KL-regularization. Therefore, to ensure a fair and direct comparison, we benchmarked our method against their respective officially released models. To demonstrate the robustness of the MixGRPO across distinct foundational models, we also followed Flow-GRPO [17] and applied the Low-Rank Adaptation (LoRA) [9] on the Stable Diffusion 3.5(SD3.5) [4]. We used HPS-v2.1 [41], Pick Score [12], and ImageReward [42] as multi-rewards, comparing Flow-DPO (offline/online) [18], and Flow-GRPO [17]. The results in Table 3 showed that MixGRPO is well-suited for the LoRA, significantly reducing training overhead while outperforming both Flow-DPO and Flow-GRPO in terms of speed and performance. The visualization results can be found in Supplementary.

4.4. Ablation Experiments

4.4.1. Sliding Window Hyperparameters

As introduced in Section 3.2, the *moving strategy*, *shift interval* τ , *window size* w and *window stride* s are parameters introduced by the SDE sliding window. We conducted ab-

Table 6. Comparison for different window size w .

w	NFE_{π_θ}	HPS-v2.1	Pick Score	ImageReward	Unified Reward
2	2	0.362	0.235	1.588	3.419
4	4	0.367	0.237	1.629	3.418
6	6	0.370	0.238	1.547	3.398

Table 7. Comparison for different window stride s .

s	HPS-v2.1	Pick Score	ImageReward	Unified Reward
1	0.367	0.237	1.629	3.418
2	0.357	0.236	1.575	3.391
3	0.370	0.236	1.578	3.404
4	0.368	0.238	1.575	3.407

Table 8. Comparison of performance across different solvers. The second-order Midpoint method achieves the best performance.

Order	Solver Type	HPS-v2.1	Pick Score	ImageReward	Unified Reward
1	/	0.367	0.236	1.570	3.403
2	Midpoint	0.358	0.237	1.578	3.407
	Heun	0.362	0.233	1.488	3.399
3	/	0.359	0.234	1.512	3.387

lation experiments on each of them.

For the moving strategy, we compared three approaches: *frozen*, where the window remains stationary; *random*, where a random window position is selected at each iteration; and *progressive*, where the sliding window moves incrementally with the denoising steps. For the *progressive* strategy, we tested different scheduling strategies where the interval τ initially starts at 25 but changes with training iterations. As shown in Table 4, the results indicate that under the *progressive* strategy, either exponential decay or constant scheduling strategies are optimal. For the *shift interval* τ , 25 is the optimal setting (See Table 5). The number of inferences for π_θ increases with the growth of the window size w , leading to greater time overhead. We compared different settings of w , and the results are shown in Table 6. Ultimately, we selected $w = 4$ as a balanced setting between overhead and performance. For the *window stride* s , we found through experimentation that $s = 1$ is the optimal choice, as shown in Table 7.

In practice, the optimal settings are applicable not only to Flux [13] but also to Stable Diffusion 3.5 [4]. Moreover, the model can maintain its optimal generation performance within a controllable range of parameter adjustments. This demonstrates the robustness of the sliding-window optimization scheduling strategy.

4.4.2. High Order ODE Solver

MixGRPO-Flash, which incorporates a high-order ODE solver to accelerate the sampling process of the reference model, achieves an effective trade-off between speed and performance. For MixGRPO-Flash, we first conducted ablation experiments on the order of the solver, using DPM-Solver++ [22] as the high-order solver with the *progressive* strategy. The results, as shown in Table 8, indicate that the second-order mid-point method is the optimal setting, optimizing the most human preference alignment metrics while simultaneously accelerating the process.

Table 9. Comparison about different sampling steps of the reference model. MixGRPO-Flash and MixGRPO-Flash* all achieve a balance between overhead and performance.

Method	Sampling Overhead		Human Preference Alignment			
	$NFE_{\pi_{\text{ref}}}$	Time per Image (s)	HPS-v2.1	Pick Score	ImageReward	Unified Reward
DanceGRPO	25	9.301	0.334	0.225	1.335	3.374
MixGRPO-Flash	19 (Avg)	7.343	0.357	0.236	1.564	3.394
	16 (Avg)	6.426	0.362	0.237	1.578	3.407
	13 (Avg)	5.453	0.344	0.229	1.447	3.363
MixGRPO-Flash*	12	4.859	0.353	0.230	1.588	3.396
	10	4.214	0.359	0.234	1.548	3.430
	8	3.789	0.357	0.232	1.624	3.402

Then we compared two acceleration approaches. One is MixGRPO-Flash, and the other is MixGRPO-Flash*. Both utilize a second-order ODE solver for acceleration, but they differ in their sliding-window moving strategies. The quantitative results are presented in Table 9. MixGRPO-Flash requires the window to move throughout the training process, resulting in a smaller portion of the ODE being accelerated compared to MixGRPO-Flash*. Consequently, MixGRPO-Flash* not only achieves a higher degree of acceleration for the reference model but also yields superior results in the ImageReward [42] and Unified Reward [38] metrics.

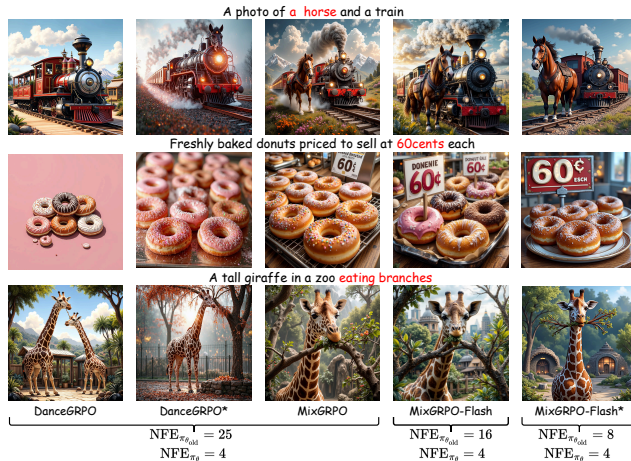


Figure 4. Qualitative results of MixGRPO-Flash. As the training overhead is reduced, generated images maintain high quality.

5. Limitation

A key limitation of GRPO is that its performance ceiling is inherently tied to the capability of the reward model. Specifically, when a reward model is not sufficiently powerful to provide a comprehensive assessment of image quality, the GRPO algorithm is prone to reward hacking, particularly in the later stages of training. As confirmed by several studies [23, 39, 40], reward hacking is fundamentally an issue stemming from the limitations of the reward model and is less attributable to the RL algorithm itself. In this context, the primary focus of MixGRPO is not to overcome the reward model’s limitations, but rather to explore how to achieve faster convergence and superior performance under the guidance of existing, imperfect reward models. Looking

ahead, while the ultimate performance is contingent upon the reward model’s quality, we plan to explore and train more powerful reward models as a direction for future work.

6. Conclusion

In this work, we have presented MixGRPO, a novel hybrid ODE-SDE framework for improving GRPO training efficiency and performance. We have proposed a strategy to confine optimization to a dynamic stochastic interval managed by a sliding window. This guides the optimization process from broad exploration to fine-grained refinement, thus enhancing performance. Experiments demonstrate that MixGRPO has achieved superior performance in both single-reward and multi-reward settings while substantially reducing overhead. Furthermore, we have presented MixGRPO-Flash, a variant offering a flexible trade-off between performance and computational cost.

References

- [1] Michael S Albergo, Nicholas M Boffi, and Eric Vandenberg. Stochastic interpolants: A unifying framework for flows and diffusions. *arXiv preprint arXiv:2303.08797*, 2023. 3, 1
- [2] Ron Amit, Ron Meir, and Kamil Ciosek. Discount factor as a regularizer in reinforcement learning. In *International conference on machine learning*, pages 269–278. PMLR, 2020. 2, 5
- [3] Kevin Black, Michael Janner, Yilun Du, Ilya Kostrikov, and Sergey Levine. Training diffusion models with reinforcement learning. *arXiv preprint arXiv:2305.13301*, 2023. 2
- [4] Patrick Esser, Sumith Kulal, Andreas Blattmann, Rahim Entezari, Jonas Müller, Harry Saini, Yam Levi, Dominik Lorenz, Axel Sauer, Frederic Boesel, et al. Scaling rectified flow transformers for high-resolution image synthesis. In *Forty-first international conference on machine learning*, 2024. 3, 5, 7, 8
- [5] Ying Fan and Kangwook Lee. Optimizing ddp sampling with shortcut fine-tuning. *arXiv preprint arXiv:2301.13362*, 2023. 2
- [6] Ying Fan, Olivia Watkins, Yuqing Du, Hao Liu, Moonkyung Ryu, Craig Boutilier, Pieter Abbeel, Mohammad Ghavamzadeh, Kangwook Lee, and Kimin Lee. Dpok: Reinforcement learning for fine-tuning text-to-image diffusion models. *Advances in Neural Information Processing Systems*, 36:79858–79885, 2023. 2
- [7] Ruiqi Gao, Emiel Hoogeboom, Jonathan Heek, Valentin De Bortoli, Kevin P. Murphy, and Tim Salimans. Diffusion meets flow matching: Two sides of the same coin. 2024. 3, 6
- [8] Jonathan Ho, Ajay Jain, and Pieter Abbeel. Denoising diffusion probabilistic models. *Advances in neural information processing systems*, 33:6840–6851, 2020. 2
- [9] Edward J Hu, Yelong Shen, Phillip Wallis, Zeyuan Allen-Zhu, Yuanzhi Li, Shean Wang, Lu Wang, Weizhu Chen, et al. Lora: Low-rank adaptation of large language models. *ICLR*, 1(2):3, 2022. 7
- [10] Hao Hu, Yiqin Yang, Qianchuan Zhao, and Chongjie Zhang. On the role of discount factor in offline reinforcement learning. In *International conference on machine learning*, pages 9072–9098. PMLR, 2022. 2, 5
- [11] Tero Karras, Miika Aittala, Timo Aila, and Samuli Laine. Elucidating the design space of diffusion-based generative models. *Advances in neural information processing systems*, 35:26565–26577, 2022. 5
- [12] Yuval Kirstain, Adam Polyak, Uriel Singer, Shahbuland Matiana, Joe Penna, and Omer Levy. Pick-a-pic: An open dataset of user preferences for text-to-image generation. *Advances in Neural Information Processing Systems*, 36:36652–36663, 2023. 2, 5, 6, 7, 3, 4
- [13] Black Forest Labs. Flux. <https://github.com/black-forest-labs/flux>, 2024. 6, 8
- [14] Kimin Lee, Hao Liu, Moonkyung Ryu, Olivia Watkins, Yuqing Du, Craig Boutilier, Pieter Abbeel, Mohammad Ghavamzadeh, and Shixiang Shane Gu. Aligning text-to-image models using human feedback. *arXiv preprint arXiv:2302.12192*, 2023. 2
- [15] Zhanhao Liang, Yuhui Yuan, Shuyang Gu, Bohan Chen, Tiankai Hang, Mingxi Cheng, Ji Li, and Liang Zheng. Aesthetic post-training diffusion models from generic preferences with step-by-step preference optimization. In *Proceedings of the Computer Vision and Pattern Recognition Conference*, pages 13199–13208, 2025. 2
- [16] Yaron Lipman, Ricky TQ Chen, Heli Ben-Hamu, Maximilian Nickel, and Matt Le. Flow matching for generative modeling. *arXiv preprint arXiv:2210.02747*, 2022. 3, 4
- [17] Jie Liu, Gongye Liu, Jiajun Liang, Yangguang Li, Jiaheng Liu, Xintao Wang, Pengfei Wan, Di Zhang, and Wanli Ouyang. Flow-grpo: Training flow matching models via online rl. *arXiv preprint arXiv:2505.05470*, 2025. 1, 2, 3, 4, 7
- [18] Jie Liu, Gongye Liu, Jiajun Liang, Ziyang Yuan, Xiaokun Liu, Mingwu Zheng, Xiele Wu, Qiulin Wang, Wenyu Qin, Menghan Xia, et al. Improving video generation with human feedback. *arXiv preprint arXiv:2501.13918*, 2025. 1, 7
- [19] Xingchao Liu, Chengyue Gong, and Qiang Liu. Flow straight and fast: Learning to generate and transfer data with rectified flow. *arXiv preprint arXiv:2209.03003*, 2022. 4, 1
- [20] Ilya Loshchilov and Frank Hutter. Decoupled weight decay regularization. *arXiv preprint arXiv:1711.05101*, 2017. 6
- [21] Cheng Lu, Yuhao Zhou, Fan Bao, Jianfei Chen, Chongxuan Li, and Jun Zhu. Dpm-solver: A fast ode solver for diffusion probabilistic model sampling in around 10 steps. *Advances in Neural Information Processing Systems*, 35:5775–5787, 2022. 2, 6
- [22] Cheng Lu, Yuhao Zhou, Fan Bao, Jianfei Chen, Chongxuan Li, and Jun Zhu. Dpm-solver++: Fast solver for guided sampling of diffusion probabilistic models. *arXiv preprint arXiv:2211.01095*, 2022. 2, 6, 8, 1
- [23] Kei Nishimura-Gasparian, Isaac Dunn, Henry Sleight, Miles Turpin, Evan Hubinger, Carson Denison, and Ethan Perez. Reward hacking behavior can generalize across tasks—ai alignment forum. In *AI Alignment Forum*, 2024. 8
- [24] Bernt Øksendal. Stochastic differential equations. In *Stochastic differential equations: an introduction with applications*, pages 38–50. Springer, 2003. 3, 1
- [25] Long Ouyang, Jeffrey Wu, Xu Jiang, Diogo Almeida, Carroll Wainwright, Pamela Mishkin, Chong Zhang, Sandhini Agarwal, Katarina Slama, Alex Ray, et al. Training language models to follow instructions with human feedback. *Advances in neural information processing systems*, 35:27730–27744, 2022. 1
- [26] Silviu Pitis. Rethinking the discount factor in reinforcement learning: A decision theoretic approach. In *Proceedings of the AAAI conference on artificial intelligence*, pages 7949–7956, 2019. 2, 5
- [27] Alec Radford, Jong Wook Kim, Chris Hallacy, Aditya Ramesh, Gabriel Goh, Sandhini Agarwal, Girish Sastry, Amanda Askell, Pamela Mishkin, Jack Clark, et al. Learning transferable visual models from natural language supervision. In *International conference on machine learning*, pages 8748–8763. PMLR, 2021. 6

- [28] Hannes Risken and Hannes Risken. *Fokker-planck equation*. Springer, 1996. 3
- [29] Robin Rombach, Andreas Blattmann, Dominik Lorenz, Patrick Esser, and Björn Ommer. High-resolution image synthesis with latent diffusion models. In *Proceedings of the IEEE/CVF conference on computer vision and pattern recognition*, pages 10684–10695, 2022. 1
- [30] Tim Salimans and Jonathan Ho. Progressive distillation for fast sampling of diffusion models. *arXiv preprint arXiv:2202.00512*, 2022. 2
- [31] John Schulman, Filip Wolski, Prafulla Dhariwal, Alec Radford, and Oleg Klimov. Proximal policy optimization algorithms. *arXiv preprint arXiv:1707.06347*, 2017. 2
- [32] Zhihong Shao, Peiyi Wang, Qihao Zhu, Runxin Xu, Junxiao Song, Xiao Bi, Haowei Zhang, Mingchuan Zhang, YK Li, Y Wu, et al. Deepseekmath: Pushing the limits of mathematical reasoning in open language models. *arXiv preprint arXiv:2402.03300*, 2024. 1, 4
- [33] Jiaming Song, Chenlin Meng, and Stefano Ermon. Denoising diffusion implicit models. *arXiv preprint arXiv:2010.02502*, 2020. 2, 4
- [34] Yang Song, Jascha Sohl-Dickstein, Diederik P Kingma, Abhishek Kumar, Stefano Ermon, and Ben Poole. Score-based generative modeling through stochastic differential equations. *arXiv preprint arXiv:2011.13456*, 2020. 2, 3, 1
- [35] Chengzhuo Tong, Ziyu Guo, Renrui Zhang, Wenyu Shan, Xinyu Wei, Zhenghao Xing, Hongsheng Li, and Pheng-Ann Heng. Delving into rl for image generation with cot: A study on dpo vs. grpo. *arXiv preprint arXiv:2505.17017*, 2025. 2
- [36] Bram Wallace, Meihua Dang, Rafael Rafailov, Linqi Zhou, Aaron Lou, Senthil Purushwalkam, Stefano Ermon, Caiming Xiong, Shafiq Joty, and Nikhil Naik. Diffusion model alignment using direct preference optimization. In *Proceedings of the IEEE/CVF Conference on Computer Vision and Pattern Recognition*, pages 8228–8238, 2024. 2
- [37] Feng Wang and Zihao Yu. Coefficients-preserving sampling for reinforcement learning with flow matching. *arXiv preprint arXiv:2509.05952*, 2025. 2, 3, 4
- [38] Yibin Wang, Yuhang Zang, Hao Li, Cheng Jin, and Jiaqi Wang. Unified reward model for multimodal understanding and generation. *arXiv preprint arXiv:2503.05236*, 2025. 2, 6, 8
- [39] Lilian Weng. Reward hacking in reinforcement learning. *lilianweng.github.io*, 2024. 8
- [40] Jie Wu, Yu Gao, Zilyu Ye, Ming Li, Liang Li, Hanzhong Guo, Jie Liu, Zeyue Xue, Xiaoxia Hou, Wei Liu, et al. Rewarddance: Reward scaling in visual generation. *arXiv preprint arXiv:2509.08826*, 2025. 8
- [41] Xiaoshi Wu, Yiming Hao, Keqiang Sun, Yixiong Chen, Feng Zhu, Rui Zhao, and Hongsheng Li. Human preference score v2: A solid benchmark for evaluating human preferences of text-to-image synthesis. *arXiv preprint arXiv:2306.09341*, 2023. 2, 6, 7, 3, 4
- [42] Jiazheng Xu, Xiao Liu, Yuchen Wu, Yuxuan Tong, Qinkai Li, Ming Ding, Jie Tang, and Yuxiao Dong. Imagereward: Learning and evaluating human preferences for text-to-image generation. *Advances in Neural Information Processing Systems*, 36:15903–15935, 2023. 1, 2, 5, 6, 7, 8, 3, 4
- [43] Zeyue Xue, Jie Wu, Yu Gao, Fangyuan Kong, Lingting Zhu, Mengzhao Chen, Zhiheng Liu, Wei Liu, Qiushan Guo, Weilin Huang, et al. Dancegrpo: Unleashing grpo on visual generation. *arXiv preprint arXiv:2505.07818*, 2025. 1, 2, 3, 6, 7
- [44] GitHub User yifan123. Discussion on flow-grpo issue 7. https://github.com/yifan123/flow_grpo/issues/#issuecomment-2870678379, 2025. Accessed: 2025-05-12. 2
- [45] Tianwei Yin, Michaël Gharbi, Richard Zhang, Eli Shechtman, Fredo Durand, William T Freeman, and Taesung Park. One-step diffusion with distribution matching distillation. In *Proceedings of the IEEE/CVF conference on computer vision and pattern recognition*, pages 6613–6623, 2024. 2
- [46] Huizhuo Yuan, Zixiang Chen, Kaixuan Ji, and Quanquan Gu. Self-play fine-tuning of diffusion models for text-to-image generation. *Advances in Neural Information Processing Systems*, 37:73366–73398, 2024. 2
- [47] Wenliang Zhao, Lujia Bai, Yongming Rao, Jie Zhou, and Jiwen Lu. Unipc: A unified predictor-corrector framework for fast sampling of diffusion models. *Advances in Neural Information Processing Systems*, 36:49842–49869, 2023. 2, 6
- [48] Kaiwen Zheng, Cheng Lu, Jianfei Chen, and Jun Zhu. Dpm-solver-v3: Improved diffusion ode solver with empirical model statistics. In *Thirty-seventh Conference on Neural Information Processing Systems*, 2023. 2, 6
- [49] Yang Zhou, Hao Shao, Letian Wang, Zhuofan Zong, Hongsheng Li, and Steven L Waslander. Drivinggen: A comprehensive benchmark for generative video world models in autonomous driving. *arXiv preprint arXiv:2601.01528*, 2026. 1

MixGRPO: Unlocking Flow-based GRPO Efficiency with Mixed ODE-SDE

Supplementary Material

7. Proof of Convergence for Mixed ODE-SDE Sampling

To prove that the mixed ODE-SDE sampling method in Eq. (7) has the same convergence as Eq. (2), which uses only ODE sampling, referencing [34], we approach this from the perspective of distribution evolution, where the distribution at each time step, e.g., $\frac{\partial q_t(\mathbf{x})}{\partial t}$ must be the same. Let the interval for SDE be defined as $S = [t_l, t_r) \in [0, 1)$. Along the denoising direction, when the same initial Gaussian noise distribution $q_0(\mathbf{x}_0)$ is given, the probability distribution evolution in the ODE interval preceding the SDE is completely identical. The key point is whether the distribution evolution of the SDE within the interval S is completely equivalent to that of the ODE. If they are equivalent, then the ODE interval following the SDE will naturally be equivalent to using only ODE sampling. Next, we will provide a detailed proof for this key point.

Consider the SDE Eq. (3) in the interval S , which possesses the following form:

$$d\mathbf{x} = [f(\mathbf{x}, t) - g^2(t)\nabla_{\mathbf{x}} \log q_t(\mathbf{x})]dt + g(t)d\mathbf{w}, \quad t \in S. \quad (12)$$

The marginal probability density $q_t(\mathbf{x}_t)$ evolves according to Kolmogorov's equation (Fokker-Planck equation) [24]

$$\begin{aligned} \frac{\partial q_t(\mathbf{x})}{\partial t} = & -\nabla_{\mathbf{x}} \cdot [(f(\mathbf{x}, t) - g^2(t)\nabla_{\mathbf{x}} \log q_t(\mathbf{x}))q_t(\mathbf{x})] \\ & + \frac{1}{2}g^2(t)\nabla_{\mathbf{x}}^2 q_t(\mathbf{x}) \end{aligned} \quad (13)$$

According to the definition of the Laplace operator $\nabla^2 h \equiv \nabla \cdot \nabla(h)$ and $\nabla_{\mathbf{x}} \log q_t(\mathbf{x}) = \frac{\nabla q_t(\mathbf{x})}{q_t(\mathbf{x})}$, we can obtain:

$$\begin{aligned} \frac{\partial q_t(\mathbf{x})}{\partial t} = & -\nabla_{\mathbf{x}} \cdot [f(\mathbf{x}, t)q_t(\mathbf{x}) - g^2(t)\nabla_{\mathbf{x}} q_t(\mathbf{x})] \\ & + \frac{1}{2}g^2(t)\nabla_{\mathbf{x}}^2 q_t(\mathbf{x}) \\ = & -\nabla_{\mathbf{x}} \cdot [f(\mathbf{x}, t)q_t(\mathbf{x}) - \frac{1}{2}g^2(t)\nabla_{\mathbf{x}} q_t(\mathbf{x})] \\ = & -\nabla_{\mathbf{x}} \cdot \underbrace{\left[(f(\mathbf{x}, t) - \frac{1}{2}g^2(t)\nabla_{\mathbf{x}} \log q_t(\mathbf{x})) q_t(\mathbf{x}) \right]}_{f_{\text{ODE}}(\mathbf{x}, t)}. \end{aligned} \quad (14)$$

The Eq. (14) is indeed the Fokker-Planck equation of the ODE Eq. (2). Therefore, within the interval S , the distribution evolution of SDE and ODE sampling is consistent.

8. DPM-Solver++ for Rectified Flow

For clarity and to avoid ambiguity between continuous time and discrete steps, we adopt the following notation in this

section. We denote the discrete time steps by an index $i \in \{0, 1, \dots, T-1\}$, where T is the total number of sampling steps. The continuous time corresponding to step i is denoted by $t_i = \frac{i}{T} \in [0, 1)$.

The DPM-Solver++ algorithm [22] is originally designed for the \mathbf{x}_0 -prediction diffusion model [29], where the model outputs the denoised feature \mathbf{x}_0 based on the noisy feature \mathbf{x}_{t_i} , the time condition t_i and the text condition c . According to the definition of Rectified Flow (RF) [19], there is the following transfer equation:

$$\mathbf{x}_{t_i} = t_i \mathbf{x}_1 + (1 - t_i) \mathbf{x}_0. \quad (15)$$

According to the theory of stochastic interpolation [1], RF effectively approximates $\mathbf{x}_1 - \mathbf{x}_0$ by modeling \mathbf{v}_{t_i} :

$$\mathbf{v}_{t_i} = \mathbf{x}_1 - \mathbf{x}_0. \quad (16)$$

Based on Eq. (15) and Eq. (16), we obtain the following relationship:

$$\mathbf{x}_0 = \mathbf{x}_{t_i} - \mathbf{v}_{t_i} t_i. \quad (17)$$

By using a neural network for approximation, we establish the relationship between RF and the \mathbf{x}_0 -prediction model:

$$\mathbf{x}_\theta(\mathbf{x}_i, t_i, c) = \mathbf{x}_i - \mathbf{v}_\theta(\mathbf{x}_i, t_i, c) \cdot t_i. \quad (18)$$

Taking the multistep second-order DPMSolver++ as an example (see Algorithm 2 in [22]), we derive the corrected \mathbf{x}_θ for the RF sampling process as \mathbf{D}_i :

$$\begin{aligned} \mathbf{D}_i \leftarrow & \left(1 + \frac{h_i}{2h_{i-1}} \right) (\mathbf{x}_{i-1} - \mathbf{v}_\theta(\mathbf{x}_{i-1}, t_{i-1}, c) \cdot t_{i-1}) \\ & - \frac{h_i}{2h_{i-1}} (\mathbf{x}_{i-2} - \mathbf{v}_\theta(\mathbf{x}_{i-2}, t_{i-2}, c) \cdot t_{i-2}), \end{aligned} \quad (19)$$

where $h_i = \lambda_{t_i} - \lambda_{t_{i-1}}$. The continuous time t_i corresponds to the discrete step i over a total of T sampling steps. The term λ_{t_i} is the log-signal-to-noise-ratio (log-SNR) and is defined in RF as:

$$\lambda_{t_i} := \log \left(\frac{1 - t_i}{t_i} \right). \quad (20)$$

Based on the exact discretization formula for the probability flow ODE proposed in DPM-Solver++ (Eq. (9) in [22]), we can derive the final transfer equation:

$$\mathbf{x}_i \leftarrow \frac{t_i}{t_{i-1}} \mathbf{x}_{i-1} - (1 - t_i) \left(e^{-h_i} - 1 \right) \mathbf{D}_i, \quad 1 \leq i < T. \quad (21)$$

9. MixGRPO-Flash Algorithm

MixGRPO-Flash Algorithm 2 accelerates the ODE sampling that does not contribute to the calculation of the policy ratio after the sliding window by using DPM-Solver++ in the Eq. (21). We introduce a compression rate \tilde{r} such that the ODE sampling after the window only requires $(T - l - w)\tilde{r}$ time steps. And the total time-steps is $\tilde{T} = l + w + (T - l - w)\tilde{r}$. The final algorithm is as follows:

Note that when using MixGRPO-Flash*, the frozen strategy is applied, with the left boundary of the sliding window $l \equiv 0$. The theoretical speedup of the training-time sampling can be described as follows:

$$S = \frac{T}{w + (T - w)\tilde{r}}. \quad (22)$$

For MixGRPO-Flash, since the sliding window moves according to the progressive strategy during training, the average speedup can be expressed in the following form:

$$S = \frac{T}{\mathbb{E}_l(w + l + [(T - w - l)\tilde{r}])} < \frac{T}{w + (T - w)\tilde{r}}. \quad (23)$$

10. Hybrid Inference for Solving Reward Hacking

As discussed in Section 5, reward hacking stems from the limited evaluation capabilities of the reward model. To address reward hacking and improve visualization, we employ the hybrid inference strategy from [44], which uses the post-trained model for low-SNR (signal-to-noise ratio) steps and the original model for high-SNR steps during inference-time sampling. In our experiments, we also applied hybrid inference to the other baseline models to ensure a fair and consistent comparison.

We employ hybrid inference and introduce the hybrid percent p_{mix} . This means that the initial, high-SNR $p_{\text{mix}}T$ denoising steps, are handled by the model trained with GRPO, while the remaining denoising process is finished by the original model. Table 10 and Figure 5 respectively illustrate the changes in performance and images as p_{mix} increases under the multi-rewards training scenario. The experimental results demonstrate that $p_{\text{mix}} = 80\%$ is an optimal empirical value that effectively mitigates hacking while maximizing alignment with human preferences.



Figure 5. Qualitative comparison with different hybrid inference percentages. We found 80% to be the optimal value, as it maximizes image quality without causing over-optimization.

Algorithm 2 MixGRPO-Flash Training Process

Require: initial policy model π_θ ; reward models $\{R_k\}_{k=1}^K$; prompt dataset \mathcal{C} ; total sampling steps \tilde{T} ; number of samples per prompt N ; ODE compression rate \tilde{r}

Require: sliding window $W(l)$, window size w , shift interval τ , window stride s

- 1: Init left boundary of $W(l)$: $l \leftarrow 0$
- 2: **for** training iteration $m = 1$ **to** M **do**
- 3: Sample batch prompts $\mathcal{C}_b \sim \mathcal{C}$
- 4: Update old policy model: $\pi_{\theta_{\text{old}}} \leftarrow \pi_\theta$
- 5: **for** each prompt $\mathbf{c} \in \mathcal{C}_b$ **do**
- 6: Init the same noise $\mathbf{x}_0 \sim \mathcal{N}(0, \mathbf{I})$
- 7: **for** generate i -th image from $i = 1$ **to** N **do**
- 8: **for** sampling timestep $t = 0$ **to** $\tilde{T} - 1$ **do**
- 9: **if** $t < l$ **then**
- 10: Use first-order ODE sampling to get \mathbf{x}_{t+1}^i
- 11: **else if** $l \leq t < l + w$ **then**
- 12: Use SDE sampling to get \mathbf{x}_{t+1}^i
- 13: **else** ▷ higher-order ODE
- 14: Use DPM-Solver++ sampling to get \mathbf{x}_{t+1}^i
- 15: **end if**
- 16: **end for**
- 17: **end for**
- 18: **for** i -th image from $i = 1$ **to** N **do**
- 19: Calculate advantage: $A_i \leftarrow \sum_{k=1}^K \frac{R(\mathbf{x}_{\tilde{T}, \mathbf{c}}^i)_k - \mu_k}{\sigma_k}$
- 20: **end for**
- 21: **for** optimization timestep $t \in W(l)$ **do**
- 22: Update policy model: $\theta \leftarrow \theta + \eta \nabla_{\theta} \mathcal{J}$
- 23: **end for**
- 24: **end for**
- 25: **if** use MixGRPO-Flash* **then** ▷ move sliding window
- 26: $l \leftarrow 0$
- 27: **else**
- 28: **if** $m \bmod \tau$ is 0 **then**
- 29: $l \leftarrow \min(l + s, T - w)$
- 30: **end if**
- 31: **end if**
- 32: **end for**

Table 10. Comparison with different hybrid inference percentages

p_{mix}	HPS-v2.1	Pick Score	ImageReward	Unified Reward
0%	0.313	0.226	1.089	3.369
20%	0.342	0.233	1.372	3.386
40%	0.356	0.235	1.539	3.395
60%	0.362	0.236	1.598	3.407
80%	0.366	0.238	1.610	3.411
100%	0.369	0.238	1.607	3.378

11. Cross-Dataset Experiments

To investigate the robustness and parameter sensitivity of the sliding window strategy in MixGRPO, we conducted a series of cross-dataset ablation studies. We established two reciprocal settings to evaluate both in-domain (ID) and out-of-domain (OOD) performance. In cross-dataset exper-

iment 1, the model was trained on the HPDV2 [41] dataset and evaluated on the test sets of HPDV2 (ID) and Pick-a-Pic v1 (OOD). In cross-dataset experiment 1, conversely, the model was trained on Pick-a-Pic v1 [12] and evaluated on the test sets of Pick-a-Pic v1 (ID) and HPDV2 (OOD). Within these settings, we ablated the key parameters of MixGRPO: **the moving strategy, shift interval τ , window size w and window stride s** . The results are presented in the Tables 11, 12, 13, 14.

As shown in Table 11, Progressive-Decay(Exp) and Progressive-Constant emerge as the top-performing moving strategies. While Progressive-Decay(Exp) consistently achieves the highest ImageReward [42] score in in-domain evaluations, Progressive-Constant demonstrates superior overall performance. Notably, the Progressive-Constant strategy consistently outperforms all others in out-of-domain tests, demonstrating its strong robustness and generalization capabilities.

The results concerning the shift interval (τ), which dictates the frequency of window movement in training iteration steps, are summarized in Table 12. Overall, the optimal performance is consistently observed at $\tau = 25$. Specifically, as τ is incrementally increased from 15 to 25, performance metrics exhibit a gradual rise across both in-domain and out-of-domain test sets. However, a crucial observation is the sharp decline in performance when the interval is extended to $\tau = 30$, with results even falling below the baseline achieved at $\tau = 15$. This trend suggests that a moderate reduction in the sliding window’s movement speed (from $\tau = 15$ to $\tau = 25$) allows the temporal behavior within the window to be sufficiently optimized. Conversely, overly slow window movement (exceeding $\tau = 25$) is prone to over-optimization at certain timesteps, causing the model’s distribution to diverge significantly from the target preferences of the reward models. The cross-dataset experiments further confirm the universality of $\tau = 25$ as the optimal setting.

The comparative results for the window size (w) are presented in Table 13. It is evident that both $w = 4$ and $w = 6$ represent optimal settings. Specifically, $w = 6$ slightly surpasses $w = 4$ only on the in-domain test set of Cross-dataset Experiment 1, and in other experiments, it only holds a marginal advantage in the HPS-v2.1 [41] score. It is crucial to note that the window size w corresponds to the number of denoising timesteps that must be optimized during each training iteration, which, in turn, is linearly correlated with the overall optimization overhead of the Reinforcement Learning (RL) process. Consequently, $w = 4$ is identified as the best compromise, offering an optimal trade-off between performance and computational efficiency. Regarding parameter sensitivity, we observe that the change in performance metrics—across both in-domain and out-of-domain tests—is relatively minimal when w varies between

2 and 6. This stability suggests that the model exhibits robust performance with respect to the window size setting. As long as the window size remains within a reasonable range (e.g., $2 \leq w \leq 6$), the model is capable of effective learning and maintaining stable performance, thereby reducing necessity for meticulous hyperparameter tuning.

The results concerning the stride (s), which defines the step size for each sliding window movement, are presented in Table 14. Considering all experimental metrics across the different datasets, a stride of $s = 1$ is identified as the optimal setting overall. It is important to note that the optimal window size of $w = 4$ was used in this experiment. With $s = 1$, the last three timesteps within the window are repeatedly optimized in the subsequent training cycle. Crucially, the experimental results indicate that this repetition leads to performance improvement. This is likely due to the nature of the high-SNR denoising process, where the initial timesteps (e.g., the first timestep in the window) are subject to a greater extent of GRPO optimization, despite the window size being set at $w = 4$. Conversely, the behavior learned during the subsequent three timesteps remains relatively under-optimized (underfitted) and thus significantly benefits from this repeated optimization. Furthermore, we observe that the highest in-domain HPS-v2.1 [41] score is achieved when $s = 3$. This localized optimal result may be attributed to the HPS-v2.1 [41] reward model’s preference alignment being relatively easier to optimize, suggesting that repeated optimization (i.e., smaller strides) could potentially induce over-optimization in this specific metric. In summary, $s = 1$ proves to be the most robust and generalizable choice across the varying experimental conditions.

12. Coefficients-Preserving Sampling

In our MixGRPO framework, introducing stochasticity during the inference phase is crucial for effective exploration in reinforcement learning. While a common practice involves the use of Stochastic Differential Equations (SDEs), we adopt Coefficients-Preserving Sampling (CPS) [37] as a more refined alternative to maintain the integrity of the probability path.

The standard SDE-based sampling, often discretized through the Euler-Maruyama method, follows the update rule:

$$\mathbf{x}_{t_{i-1}} = \mathbf{x}_{t_i} - \mathbf{v}_{t_i}(\mathbf{x}_{t_i}, t_i)\Delta t + \sqrt{2\sigma^2\Delta t}\epsilon_i, \quad \epsilon_i \sim \mathcal{N}(\mathbf{0}, \mathbf{I}) \quad (24)$$

Although this formulation provides the necessary stochasticity, it tends to inject excessive independent noise at each discretization step, resulting in "grainy" artifacts in the generated samples. As observed in our preliminary experiments, such high-frequency noise can lead to reward hacking, where reward models (e.g., Pick Score [12] or HPS-v2.1 [41]) prioritize low-level textures over structural co-

Table 11. Comparison for different moving strategies in cross-dataset experiments. The optimal setting is highlighted in green.

Strategy	Interval Schedule	Cross-dataset Experiment 1						Cross-dataset Experiment 2					
		In Domain Dataset (HPD v2)			Out-of-Domain Dataset (Pick-a-Pi v1)			In Domain Dataset (Pick-a-Pi v1)			Out-of-Domain Dataset (HPD v2)		
		HPS-v2.1	Pick Score	ImageReward	HPS-v2.1	Pick Score	ImageReward	HPS-v2.1	Pick Score	ImageReward	HPS-v2.1	Pick Score	ImageReward
Frozen	/	0.354	0.234	1.580	0.352	0.226	1.539	0.346	0.230	1.601	0.351	0.231	1.587
Random	Constant	0.365	0.237	1.513	0.361	0.230	1.512	0.349	0.227	1.524	0.343	0.225	1.530
Progressive	Decay(Linear)	0.365	0.235	1.566	0.363	0.229	1.572	0.363	0.231	1.614	0.355	0.230	1.597
	Decay(Exp)	0.360	0.239	1.632	0.364	0.232	1.612	0.361	0.234	1.628	0.358	0.230	1.584
	Constant	0.367	0.237	1.629	0.366	0.234	1.622	0.365	0.238	1.618	0.359	0.232	1.601

Table 12. Comparison for different shift intervals τ in cross-dataset experiments. The optimal setting is highlighted in green.

τ	Cross-dataset Experiment 1						Cross-dataset Experiment 2					
	In Domain Dataset (HPD v2)			Out-of-Domain Dataset (Pick-a-Pi v1)			In Domain Dataset (Pick-a-Pi v1)			Out-of-Domain Dataset (HPD v2)		
	HPS-v2.1	Pick Score	ImageReward	HPS-v2.1	Pick Score	ImageReward	HPS-v2.1	Pick Score	ImageReward	HPS-v2.1	Pick Score	ImageReward
15	0.366	0.237	1.509	0.359	0.227	1.470	0.358	0.234	1.610	0.353	0.228	1.542
20	0.366	0.238	1.610	0.360	0.228	1.619	0.361	0.237	1.615	0.357	0.233	1.588
25	0.367	0.237	1.629	0.366	0.234	1.623	0.365	0.238	1.618	0.359	0.232	1.601
30	0.350	0.229	1.589	0.348	0.221	1.585	0.355	0.234	1.609	0.351	0.229	1.509

Table 13. Comparison for different window sizes w in cross-dataset experiments. The optimal setting is highlighted in green.

w	Cross-dataset Experiment 1						Cross-dataset Experiment 2					
	In Domain Dataset (HPD v2)			Out-of-Domain Dataset (Pick-a-Pi v1)			In Domain Dataset (Pick-a-Pi v1)			Out-of-Domain Dataset (HPD v2)		
	HPS-v2.1	Pick Score	ImageReward	HPS-v2.1	Pick Score	ImageReward	HPS-v2.1	Pick Score	ImageReward	HPS-v2.1	Pick Score	ImageReward
1	0.359	0.232	1.571	0.349	0.223	1.445	0.349	0.229	1.553	0.346	0.221	1.565
2	0.366	0.235	1.618	0.363	0.230	1.614	0.363	0.234	1.597	0.359	0.230	1.585
4	0.367	0.237	1.629	0.366	0.234	1.623	0.365	0.238	1.618	0.359	0.232	1.601
6	0.370	0.238	1.624	0.364	0.232	1.620	0.366	0.237	1.608	0.362	0.232	1.594

Table 14. Comparison for different window strides s in cross-dataset experiments. The optimal setting is highlighted in green.

s	Cross-dataset Experiment 1						Cross-dataset Experiment 2					
	In Domain Dataset (HPD v2)			Out-of-Domain Dataset (Pick-a-Pi v1)			In Domain Dataset (Pick-a-Pi v1)			Out-of-Domain Dataset (HPD v2)		
	HPS-v2.1	Pick Score	ImageReward	HPS-v2.1	Pick Score	ImageReward	HPS-v2.1	Pick Score	ImageReward	HPS-v2.1	Pick Score	ImageReward
1	0.367	0.237	1.629	0.366	0.234	1.623	0.364	0.238	1.618	0.359	0.232	1.601
2	0.357	0.236	1.575	0.357	0.233	1.587	0.363	0.234	1.574	0.354	0.231	1.591
3	0.370	0.236	1.578	0.364	0.230	1.579	0.368	0.237	1.586	0.358	0.228	1.585
4	0.368	0.238	1.575	0.349	0.224	1.573	0.366	0.231	1.566	0.357	0.225	1.568

herence, thereby hindering the convergence of RL optimization.

To address these issues, we utilize CPS [37], which reformulates the transition process by drawing inspiration from DDIM [33] framework. The update rule for CPS [37] is defined as:

$$\mathbf{x}_{t_{i-1}} = \frac{1 - t_{i-1}}{1 - t_i} \mathbf{x}_{t_i} + \left(t_{i-1} - \frac{1 - t_{i-1}}{1 - t_i} t_i \right) \mathbf{v}_{t_i} + \sigma_{t_i} \epsilon_i \quad (25)$$

The core advantage of CPS [37] lies in its strategic construction of coefficients for \mathbf{x}_{t_i} and \mathbf{v}_{t_i} , which preserves the linear interpolation structure of Flow Matching while introducing controlled stochasticity via σ_{t_i} . By effectively eliminating sampling artifacts inherent in SDE-based methods, CPS [37] yields cleaner images that provide more reliable feedback for MixGRPO. In our implementation, we set $NFE_{\pi_{\theta_{ot,d}}} = 25$, window size $w = 4$, and window stride $s = 1$ with fixed initial noise, employing HPS-v2.1 [41], Pick Score [12], and ImageReward [42] as multi-reward metrics. Both the original SDE sampling and CPS [37] sampling were trained for 300 steps and evaluated on the HPDv2 dataset [41]. As demonstrated in Table 15, the integration of CPS [37] leads to superior performance across all reward metrics, with qualitative comparisons in Figure 9

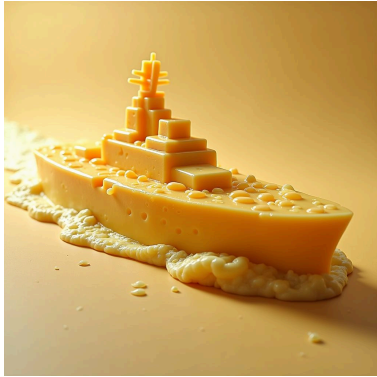
further illustrating its enhanced visual fidelity.

Table 15. Comparison with CPS sampling

Method	Pick Score	ImageReward	HPS-v2.1
FLUX	0.2265	1.0883	0.3126
MixGRPO-SDE	0.2344	1.5901	0.3648
MixGRPO-CPS	0.2382	1.6449	0.3692

13. More Visualized Results

PROMPT: An image of an aircraft carrier made of cheese.



FLUX



DanceGRPO



MixGRPO

PROMPT: 16-year-old teenager wearing a white bear-ear hat with a smirk on their face.



FLUX



DanceGRPO



MixGRPO

PROMPT: A lemon with a McDonald's hat.



FLUX



DanceGRPO



MixGRPO

Figure 6. Comparison of the visualization results of FLUX, DanceGRPO, and MixGRPO under HPS-v2.1 as the reward model.

PROMPT: A photorealistic image from a furry fandom convention set in a biopunk era after the genetic revolution and quantum singularity.



FLUX



DanceGRPO



MixGRPO

PROMPT: a castle is in the middle of a european city



FLUX



DanceGRPO



MixGRPO

PROMPT: A detailed soft painting of a bat with golden rose flowers and amethyst stained glass in the background.



FLUX



DanceGRPO



MixGRPO

Figure 7. Comparison of the visualization results of FLUX, DanceGRPO, and MixGRPO under HPS-v2.1 and CLIP Score as multi-reward models.

PROMPT: a cute polar bear baby, digital oil painting by paul nicklen and by van gogh and monet



SD3.5



Flow-DPO(offline)



Flow-DPO(online)



Flow-GRPO



MixGRPO

PROMPT: A chocolate cake with the word "SD" written on it, professional photography, food photography



SD3.5



Flow-DPO(offline)



Flow-DPO(online)



Flow-GRPO



MixGRPO

PROMPT: a photo of a yellow sports ball and a green boat



SD3.5



Flow-DPO(offline)



Flow-DPO(online)



Flow-GRPO



MixGRPO

Figure 8. Comparison of the visualization results of SD3.5-M, offline DPO, online DPO, Flow-GRPO and MixGRPO under HPS-v2.1, Pick Score and ImageReward as multi-reward models.

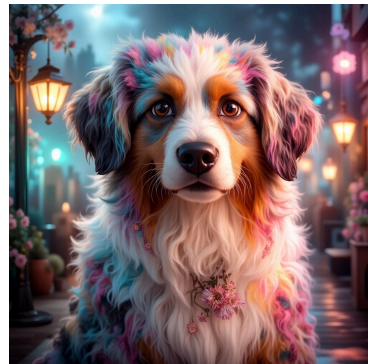
PROMPT: A key shot of an Australian Shepherd with a pastel color palette and dramatic lighting.



FLUX



MixGRPO-SDE



MixGRPO-CPS

PROMPT: Portrait of an anime princess in white and golden clothes.



FLUX



MixGRPO-SDE



MixGRPO-CPS

PROMPT: A colorful digital painting with a front view and anime-inspired vibes featuring a magical composition.



FLUX



MixGRPO-SDE



MixGRPO-CPS

Figure 9. Comparison of the visualization results of FLUX, SDE sampling and CPS sampling